pISSN 1229-3008 eISSN 2287-6251
Progress in Supercoductivity and Cryogenics
Vol.23, No.4, (2021), pp.61~69 https://doi.org/10.9714/psac.2021.23.4.061

Analysis on electrical and thermal characteristics of MI-SS racetrack coil under conduction cooling and external magnetic field

Yoon Seok Chae, Ji Hyung Kim, Huu Luong Quach, Sung Hoon Lee, and Ho Min Kim*

Department of Electrical Engineering, Jeju National University, Jeju, Korea

(Received 23 November 2021; revised or reviewed 29 December 2021; accepted 30 December 2021)

Abstract

This paper presents the analysis and experiment results on the electrical and thermal characteristics of metal insulation (MI) REBCO racetrack coil, which was wound with stainless steel (SS) tape between turn–to–turn layers, under rotating magnetic field and conduction cooling system. Although the field windings of superconducting rotating machine are designed to operate on a direct current, they may be subjected to external magnetic field due to the unsynchronized armature windings during electrical or mechanical load fluctuations. The field windings show the voltage and magnetic field fluctuations and the critical current reduction when they are exposed to an external magnetic field. Moreover, the cryogenic cooling conditions are also identified as the factors that affect the electrical and thermal characteristics of the HTS coil because the characteristic resistance changes according to the cryogenic cooling conditions. Therefore, it is necessary to investigate the effect of external magnetic field on the electrical and thermal characteristics of MI–SS racetrack coil for further development reliable HTS field windings of superconducting rotating machine. First, the major components of the experiment test (i.e., HTS racetrack coil construction, armature winding of 75 kW class induction motor, and conduction cooling system) were fabricated and assembled. Then, the MI racetrack coil was performed under liquid nitrogen bath and conduction cooling conditions to estimate the key parameters (i.e., critical current, time constant, and characteristic resistance) for the test coil in the steady state operation. Further, the test coil was charged to the target value under conduction cooling of 35 K then exposed to the rotating magnetic field, which was generated by three phrase armature windings of 75 kW class induction motor, to investigate the electrical and thermal characteristics during the transient state.

Keywords: conduction cooling system, electrical and thermal characteristics, external magnetic field, HTS rotating machine, metal insulation HTS racetrack coil

1. INTRODUCTION

Second generation (2G) high temperature superconductor (HTS) is one of the most promising candidates for the development of magnets that generate high field, such as wind power generator, nuclear magnetic resonance, and magnetic resonance imaging due to their high critical temperature, high current density under high magnetic field and high energy margin. However, one of the most fundamental issues of 2G HTS is self–protected in the unexpected quench unlike the low temperature superconductor because of low normal–zone propagation velocity [1, 2]. Therefore, detection and protection schemes have been developed for the reliable operation of HTS magnet applications. Although the no-insulation winding technique can significantly enhance the electrical and thermal stabilities for the HTS magnets, it suffers from the charging delay time (τ_d) under time varying condition, leading to limitation in the electrical applications that require fast charging such as superconducting rotating machines and superconducting magnetic energy storage systems [3–9].

Recently, the metal insulation (MI) winding technique, which employs metal insulation material between turn-to-turn layers, has been proposed to overcome slow charge–discharge rate in no–insulation coil as well as the thermal and electrical stabilities in insulated coil [10–14]. We have already reported the advantages of MI winding technique co-wound with stainless steel (SS) tapes in the form of racetrack type coils, which were applied for the field windings of 10 MW class HTS generator used in an offshore wind turbine environment, under steady and transient states [15–17]. The MI winding technique shows a good balance in terms of charging time and thermal stability during the steady and transient states. However, in the practical partially superconducting rotating machine application, the HTS field coils are subjected to an external magnetic ripple field which is generated by the armature windings. Therefore, it is essential to investigate the effect of external magnetic field on the electrical and thermal characteristics of MI racetrack coil for further development reliable large scale rotating machines.

In this study, we estimate the effect of external magnetic field, which was generated by 75 kW class induction motor, on the electrical and thermal behaviors of MI–SS racetrack type coil cooled by conduction cooling system. First, the major parameters of MI racetrack coil and 75 kW class induction motor were demonstrated. In addition, the various components of the conduction cooling system were designed and assembled. Then, the current–voltage (I–V)

* Corresponding author: hmkim@jejunu.ac.kr

tests for MI–SS racetrack coil were conducted in various cryogenic cooling conditions (i.e., liquid nitrogen (LN_2) bath and conduction cooling of 35 and 77 K) to estimate the critical current (I_c) value for the test coil. Moreover, the charging and discharging tests were performed in the LN_2 bath and conduction cooling conditions to investigate the effect of cryogenic cooling on the characteristic resistance (R_c) and τ_d for MI–SS racetrack coil. Finally, to estimate the electrical and thermal stabilities for the MI–SS racetrack coil in the transient state, the test coil was charged to the target value under conduction cooling system of 35 K then exposed to the rotating magnetic field generated by armature windings of 75 kW class induction motor. The center magnetic field and temperature of the MI–SS racetrack coil were analyzed and discussed according to the variation in external magnetic field.

2. EXPERIMENTAL SETUP

2.1. Fabrication of MI-SS racetrack coil

The major parameters of the REBCO coated conductor, which was manufactured by SuNAM Co., Ltd., and the MI–SS racetrack coil are listed in Table. 1. The width and thickness of the REBCO tape are 12.1 mm and 0.14 mm, respectively. The racetrack bobbin was made of stainless steel with outer diameter at curvature of 40 mm and straight section of 140 mm, as shown in Fig. 1. The thickness of SS tape is a factor that effect to the thermal stability of the MI–SS racetrack coil as shown in our previous study [17]. The thermal stability of the test coil increased with an increase in the thickness of SS tape used between turn–to–turn layers because thicker SS tape could absorb more joule heat energy generated by hot spot. Therefore, to increase the thermal stability for the test coil, the stainless steel thickness of 120 μm was used to fabricate the MI–SS racetrack coil. During fabrication the test coil, the winding tensions for 2G HTS and SS tapes were maintained at 10 and 5 kgf, respectively. The center bore and shoe cover were made of carbon steel (S45C) to concentrate and increase the magnetic field. The test coil was wound directly onto the center bore of SS racetrack bobbin and covered by conduction guide with oxygen–free high conductive copper (OFHC) to enhance heat transfer characteristic of conduction cooling system. Various signal sensors were used to measure the electromagnetic behavior during coil operation. Three voltage taps (V_1–V_3) were installed in every ten turns, starting from the innermost turn, and terminal voltage tap (V_t) was inserted between two terminals to measure the voltage signal in the steady and transient states. In addition, a Hall sensor was located at the center of the bobbin to measure the center magnetic field density of the test coil.

TABLE 1
PARAMETERS OF REBCO COATED CONDUCTOR AND MI-SS RACETRACK COIL.

ITEMS	UNIT	VALUES
REBCO Coated Conductor		
Manufacturer	–	SuNAM Co. Ltd
Conductor model	–	SCN12500
Conductor width	[mm]	12.1±0.1
Conductor thickness	[μm]	140±15
Max./Min. critical current	[A]	808/676
Critical temperature	[K]	91
MI-SS Racetrack Coil		
Number of turns	–	32
Insulation material	–	SS 310S
Insulation width/thickness	[mm]	12/0.12
Winding tension REBCO/SS	[kg·f]	10/5
Bobbin material	–	Copper and S45C
Conductor length	[m]	17.8
Inner radius at curvature	[mm]	40
Outer radius at curvature	[mm]	48.64
Length of straight portion	[mm]	140
Criterion voltage	[mV]	1.78
I_c @ 77 K, self-field *	[A]	239
Coil inductance	[μH]	577
R_c @ 77 K	[μΩ]	144.3
R_{ct} @ 77 K	[μΩ·cm^2]	304.7

* Measured using 1–μV/cm criterion

2.2. Fabrication of conduction cooling system integrated MI–SS racetrack coil

The MI–SS racetrack coil was placed inside the cryostat part in vertical direction as shown in Fig. 2. A pair of HTS current leads was utilized to supply an input current (I_t) into the test coil with minimizing heat intrusion. Each current lead included two 2G HTS tapes, which are the same properties with 2G HTS tape used to fabricate the test coil, and fiber reinforced plastic sheets to insulate and protect the HTS tapes. The inlet of both HTS current leads were connected to the first–stage of cryocooler. Both HTS current leads were cooled down to approximately 80 K which can transport the I_t of 1352 A (= 2 × 676 A) into the test coil. The test coil was electrically closed with two HTS current leads through OFHC terminal lead blocks. Then, they were thermally connected with the second–stage of cryocooler through conduction structure (i.e., OFHC–bars and –braided wires) to cool down the test coil to 35 K. Cernox® , DT–670 Silicon Diodes, and PT–1000 sensors were attached at various locations inside cryostat to measure the temperature, as shown in Fig. 3. In addition, to reduce thermal radiation from room temperature, thermal shield cylinder with multi–layer insulation of aluminum foil was utilized to cover all structures below the first–stage of cryocooler, as shown in Fig. 2. The configuration of 75 kW class induction motor, which was used to generate AC external magnetic field on the MI–SS racetrack coil, is shown in Fig. 4. The length of stator core, inner and outer diameters of induction motor were 214, 281 and 435 mm, respectively. The stator had 72 slots and double layer windings. During the experiment tests, the external magnetic field, which was generated by three phase

armature windings, was controlled by the frequency and current amplitude. The MI–SS racetrack coil was placed parallel to the stator to investigate the effect of the external magnetic field on the I_c and center magnetic field (B_z) of the test coil, as shown in Fig. 4. A data acquisition system was used to measure the B_z fluctuation according to variation of the external magnetic field generated by 75 kW class three phase armature windings, which was controlled by variable voltage and frequency inverter. The experiment setup for estimating the electrical and thermal characteristics of the MI–SS racetrack coil under rotating magnetic field is shown in Fig. 5.

3. RESULTS AND DISCUSSION

3.1. Cooling and vacuum test

Fig. 6 (a) shows the experimental results of vacuum and cool down temperature during the 1st and 2nd stages of cryocooler. It took around 13 and 19 hours to reach the steady state temperature for the 1st and 2nd stages, respectively. The vacuum pressure was decreased to 4.7×10^{-3} Torr using a turbo molecular pump. Then, the cryocooler started to reduce the vacuum pressure as well as temperature inside the cryostat part. In the initial hours, the temperature inside the cryostat part remained stable at room temperature. Subsequently, the temperature was maintained at 10 K under vacuum pressure of 4.06×10^{-8} Torr during around 15 hours after turning on the cryocooler, as shown in Fig. 6 (a).

Fig. 6 (b) shows the experimental result of temperature variation with respect to joule heat generation by a heater power of 50 Ω which was installed at the 2nd stage of the cryocooler. The temperature of the stage could be controlled by this heater power. However, the electrical and thermal characteristics of the test coil were not affected by the operation of the heater power because they had separate thermal link model and most of heat generation by the heater power was absorbed by the cryocooler. When the heater power was zero, the temperature of the 2nd stage remained at 10 K. To maintain the target operating temperature of 35 and 75 K for the MI–SS racetrack coil, the heater power of 9.245 and 15.125 W were respectively supplied to the cryocooler, as shown in Fig. 6 (b).

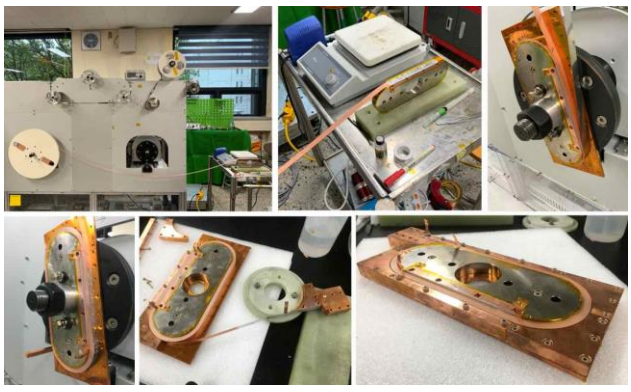

Fig. 1. Photographs of MI–SS racetrack coil.

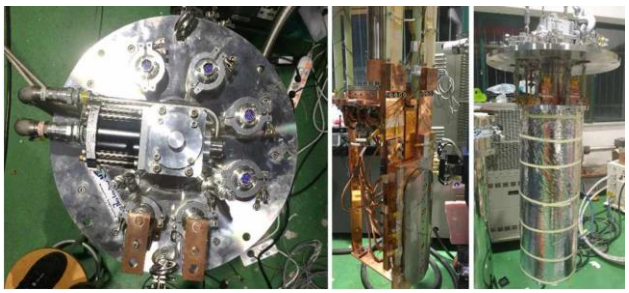

Fig. 2. Photographs of assembly MI-SS racetrack coil into the conduction cooling environment.

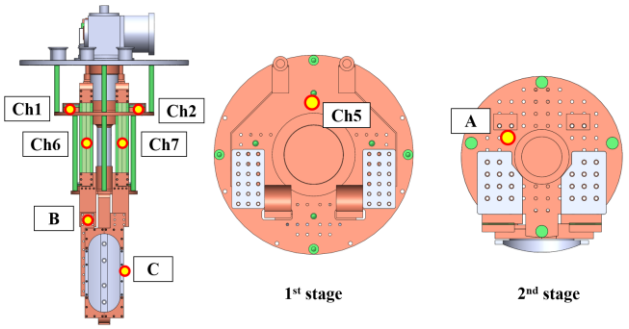

Fig. 3. Schematic drawings of the internal cryostat part with positions of temperature sensors.

Fig. 4. Photographs of assembly cryostat part into induction motor.

Fig. 5. Photographs of experiment setup.

3.2. Current-voltage test

To investigate the I_c value for MI–SS racetrack coil, the I–V tests were performed in the LN_2 bath and conduction cooling conditions. The test coil was charged with a current ramp rate of 1 A/s until the V_t increased over the V_c of 1.78 mV which was calculated by multiplying the length of HTS tape and an electric field criterion of 1–μV/cm. Then, I_t was turned off to prevent the test coil from permanent damage. Fig. 7 (a), (b), and (c) show the experiment I_c results under LN_2 bath, conduction cooling of 77 and 35 K, respectively. The I_c values of the test coil under LN_2 bath and conduction

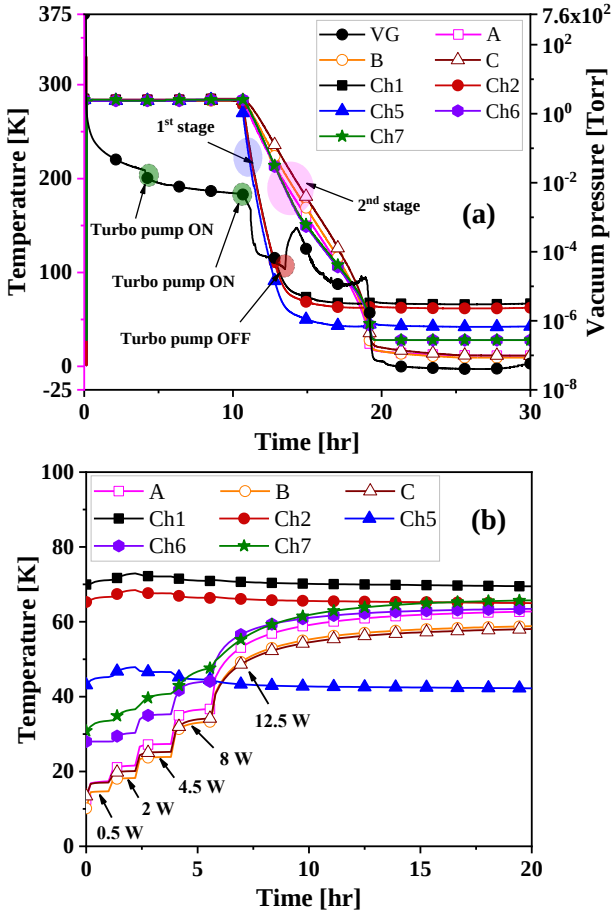

Fig. 6. Experiment results of (a) cool down temperature of cryocooler and (b) temperature variation with respect to heater power.

cooling of 77 K were respectively 239 and 236 A. However, the I_c value under conduction cooling of 35 K was assumed to be 500 A due to the limitation of power supply current. It should be noted that the I_c value under conduction cooling of 35 K may exceed 500 A because the V_t did not increase over the V_c of 1.78 mV.

The I_c value decreases significantly under a perpendicular magnetic field. Fig. 8 shows the I_c value reduction versus perpendicular flux density of 2G HTS tape manufactured by SuNAM Co., Ltd. The numerical approach was suggested to investigate the I_c value of the MI–SS racetrack coil using a three-dimensional finite element analysis (3D FEA). The test coil is charged to 500 A which is equal to the limitation value of the experimental power supply current. Fig. 9 (a) and (b) show the simulation I_c results under conduction cooling of 77 and 35 K, respectively. The I_c value is determined at the intersection point between the transport current and critical current at perpendicular flux density. The I_c value under the conduction cooling of 77 K is estimated as 245 A which are 2.45% and 3.67 % higher than those of experimental results obtained from LN_2 bath and conduction cooling condition of 77 K, respectively. In the case of conduction cooling of 35 K, the I_c value for the test coil is evaluated over 500 A which is similar to the experiment result. Overall, the simulation results were in good agreement with the experimental results, which proved that the validity of the developed 3D FEA model.

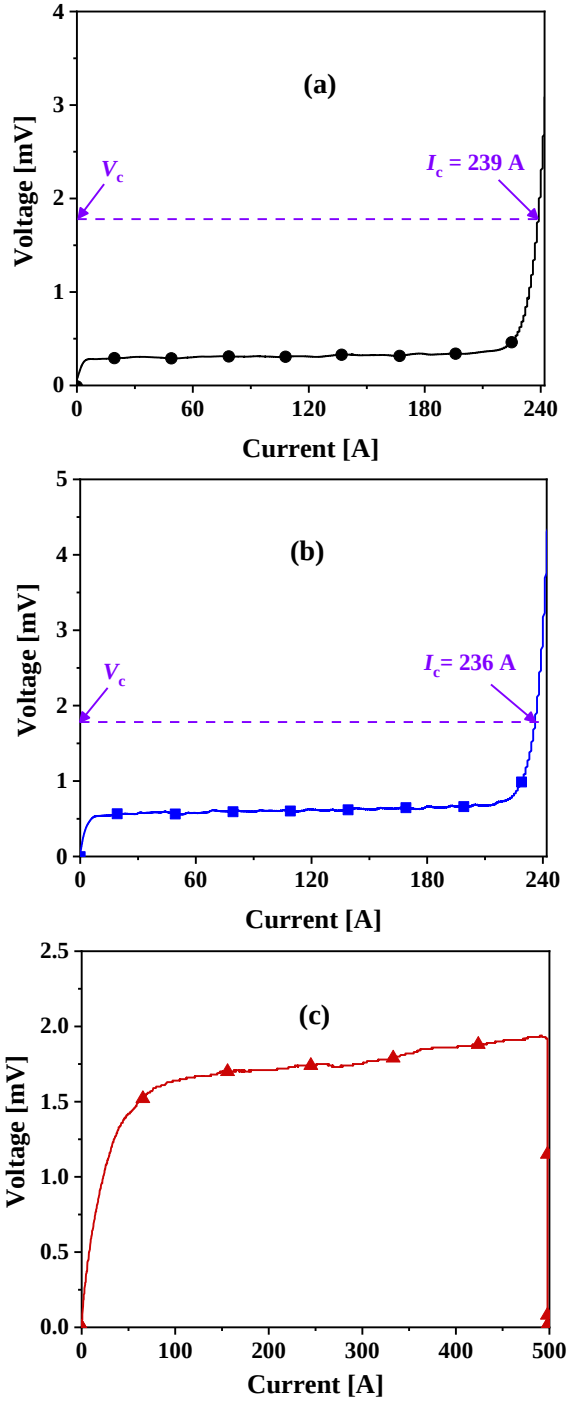

Fig. 7. Critical current results under (a) LN_2 bath, (b) conduction cooling of 77 K, and (c) conduction cooling of 35 K.

3.2. Charging and discharging test

To characterize time constant (τ) and R_c for the MI–SS racetrack coil, the charging and discharging tests were performed under the LN_2 bath and conduction cooling conditions. I_t increased up to 221 A with charging rate of 0.6 A/s under LN_2 bath and 1 A/s under conduction cooling. Then, I_t was maintained at that level so that the test coil was in a steady state condition. Finally, I_t was decreased to zero with discharging rate of 0.6 A/s under LN_2 bath and 1 A/s under conduction cooling. Fig. 10 (a), (b), and (c) show the experiment results of the I_t and V_t under LN_2 bath and

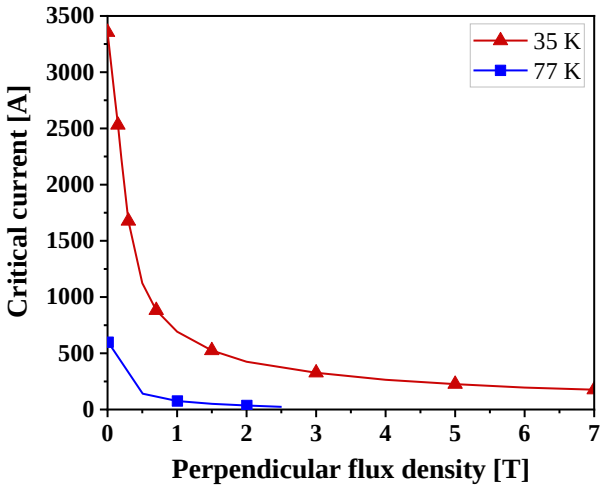

Fig. 8. Reduction of I_c value according to perpendicular flux density.

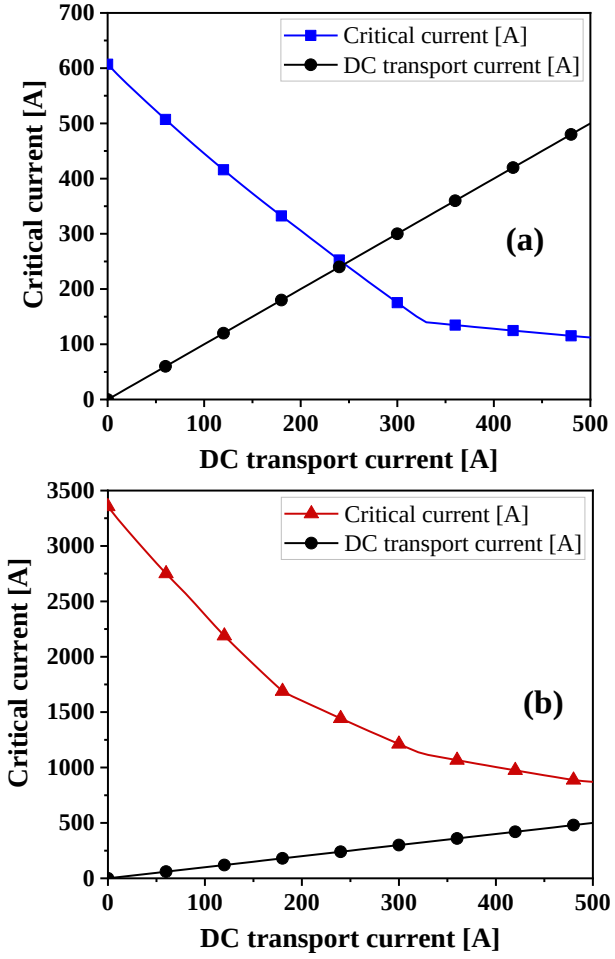

Fig. 9. Simulation critical current results under (a) conduction cooling of 77 K and (b) conduction cooling of 35 K.

conduction cooling conditions of 77 and 35 K, respectively. The τ values of the test coil under LN_2 bath and conduction cooling conditions of 77 and 35 K, which was determined at a normalized V_t value of 0.63, were 4, 4, and 9 s, respectively. The inductive voltage was determined at an average value (i.e., $V_L = [V_{max} + V_{min}]/2$) during the discharging phase due to heavy noise in the charging phase. Based on the average inductive voltage and current ramp rate (i.e., $V_L = L_c \times di/dt$), coil inductance (L_c) under LN_2 bath and conduction cooling conditions of 77 and 35 K were estimated to be 517, 609, and 581 μH, respectively. The L_c value under LN_2 bath was smaller than those of conduction cooling conditions. This may be because the small current ramp rate of 0.6 A/s under LN_2 compared to 1 A/s under conduction cooling. In general, the difference in L_c value between cooling methods may be the measurement error of experiment data owing to heavy noise measured in the V_L. Therefore, we utilized the average L_c obtained from three cooling methods to estimate R_c value for the test coil. The R_c value under conduction cooling of 35 K (63.2 μΩ), which was calculated using the values of L_c and τ (i.e., $R_c = L_c/\tau$), was smaller than those of LN_2 bath (142.3 μΩ) and conduction cooling of 77 K (142.3 μΩ). These results demonstrated that the R_c decreased as the temperature cooling decreased because joule heat generation inside the MI–SS racetrack coil was effectively eliminated at low temperature. Table 2 summarizes the experiment results of τ, L_c, and R_c for MI–SS racetrack coil under the charging and discharging tests with respect to LN_2 bath and conduction cooling conditions. Fig. 11 (a) and (b) show the temperature results inside cryostat part during the charging and discharging tests under conduction cooling conditions of 77 and 35 K, respectively. The temperatures at the channel C, which measured the temperature for the test coil, were maintained approximately 77 and 35 K, implying that joule heat generation was equilibrated with conduction cooling. Fig. 12 (a), (b), and (c) show the experiment results of I_t, V_t, and B_z versus time curves under LN_2 bath and conduction cooling conditions of 77 and 35 K, respectively. As expected, the τ_d under conduction cooling of 35 K (28 s) was slower than those of LN_2 bath (18 s) and conduction cooling of 77 K (14 s). This was because the test coil under conduction cooling of 35 K could enhance heat dissipation owing to its high performance cooling, which resulted in a decrease in R_c. Thus, the conduction cooling system of 35 K can be considered as an effective method for improving the thermal stability of the test coil.

3.3. Characteristic tests under various AC rotating magnetic field

To investigate the effect of external magnetic field on the I_c characteristic of the test coil cooled by the conduction cooling system of 35 K, the transient tests were performed under various rotating magnetic field generated by three phrase armature windings. The armature current (I_a)= 28.5, 42.5, and 57.6 A_{rms} and its frequency (f_s)= 0.5, 1, and 1.5 Hz were utilized to generate the rotating magnetic fields. The numerical approach was suggested to evaluate I_c value by using the 3D FEA model. The I_c values of the test coil were 421, 416, and 413 A at I_a= 28.5 Arms and f_s= 0.5 Hz, I_a= 42.5 Arms and f_s= 1.0 Hz, and I_a= 57.6 Arms and f_s= 1.5 Hz, respectively. Although the accuracy of I_c value under conduction cooling system of 35 K cannot be obtained by the experiment test due to the limitation of the power

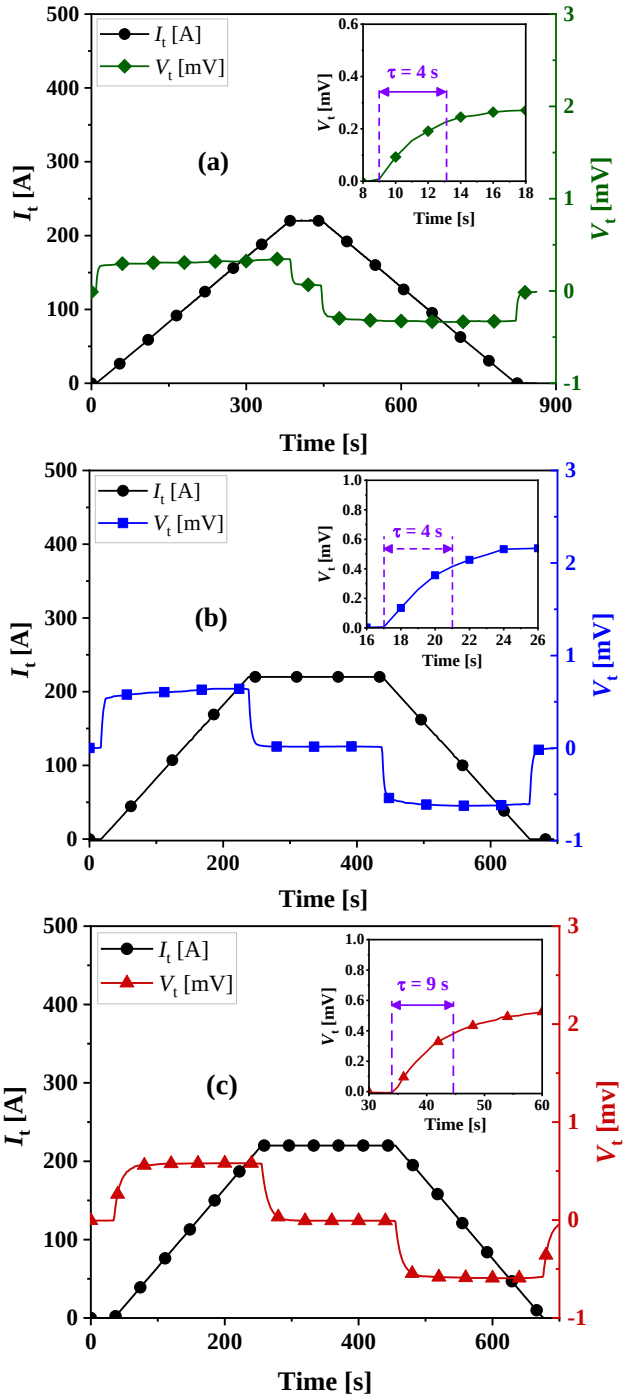

Fig. 10. Time constant results under (a) LN_2 bath, (b) conduction cooling of 77 K, and (c) conduction cooling of 35 K.

TABLE 2
EXPERIMENT RESULTS OF THE TEST COIL UNDER LN_2 BATH AND CONDUCTION COOLING CONDITIONS.

Items	Unit	Values		
Cooling approach	–	LN_2	Conduction	Conduction
Temperature	[K]	77	77	35
Inductance	[μH]	517	609	581
Average inductance	[μH]		569	
Time constant	[s]	4	4	9
Characteristic resistance	[μΩ]	142.3	142.3	63.2

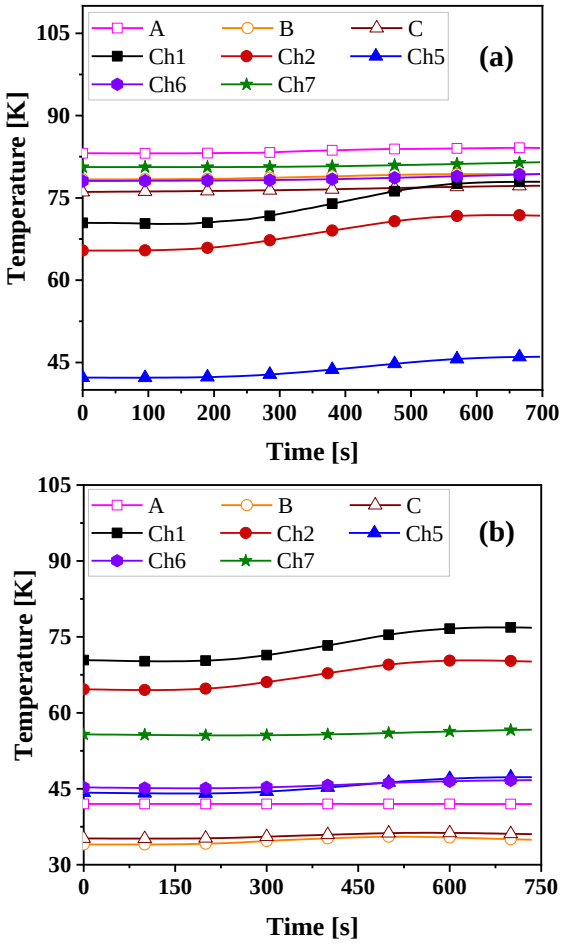

Fig. 11. Temperature results during charging and discharging test under (a) conduction cooling of 77 K, (b) conduction cooling of 35 K.

supply current, the effect of rotating magnetic field on the I_c characteristic under conduction cooling of 35 K may be investigated by the experiment test based on the trend curves of I_t and B_z values due to bypass current phenomenon. It is assumed that the I_c value is 500 A which is the maximum value of power supply current. Fig. 13 (a), (b), and (c) show the experiment results of the test coil under AC excitation in armature windings according to I_a= 28.5 A_{rms} and f_s= 0.5 Hz, I_a= 42.5 A_{rms} and f_s= 1.0 Hz, and I_a= 57.6 A_{rms} and f_s= 1.5 Hz, respectively. It is noted that the B_z curve only shows the trend of the center magnetic field for the test coil due to heavy noise. At I_a= 28.5 A_{rms} and f_s= 0.5 Hz, the magnetic field started to decrease at the I_t value of 497 A which was higher than those of I_a= 42.5 A_{rms} and f_s= 1.0 Hz (463 A) and I_a= 57.6 A_{rms} and f_s= 1.5 Hz (433 A). The experimental results demonstrated that the I_c value of the test coil was affected by the rotating magnetic field. The B_z value decreased as the strength of I_a and f_s increased. The bypass current phenomenon occurred as the external magnetic field applied to the test coil due to low R_c value.

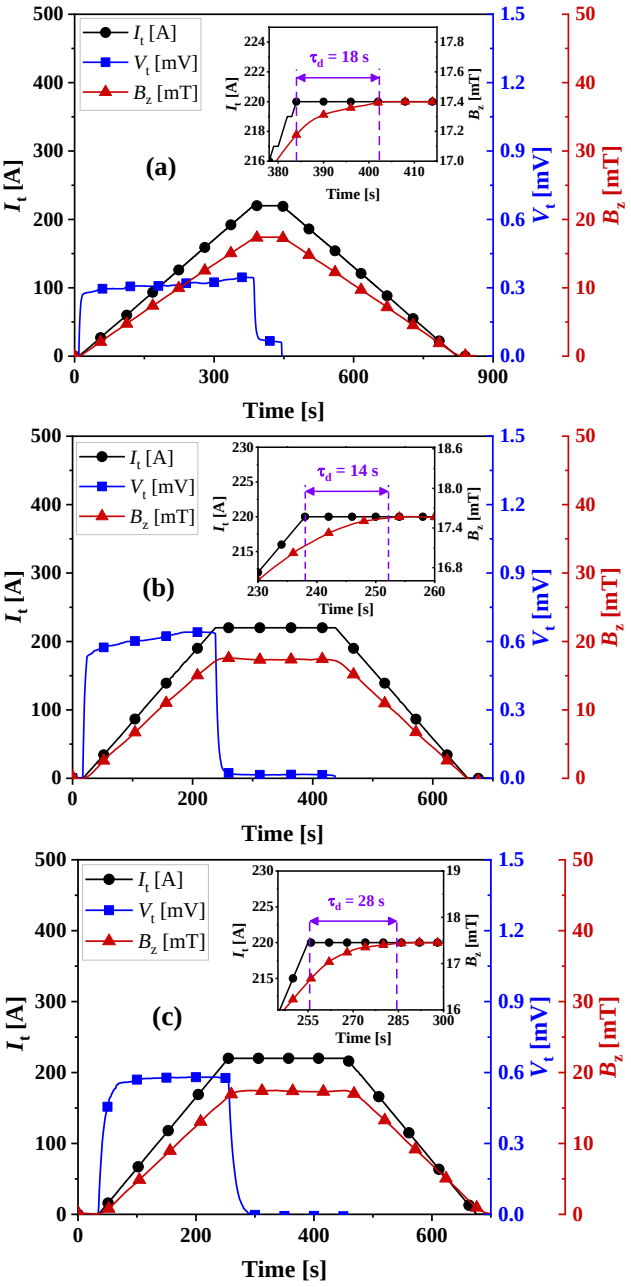

Fig. 12. Charging delay time results under (a) LN_2 bath, (b) conduction cooling of 77 K, and (c) conduction cooling of 35 K.

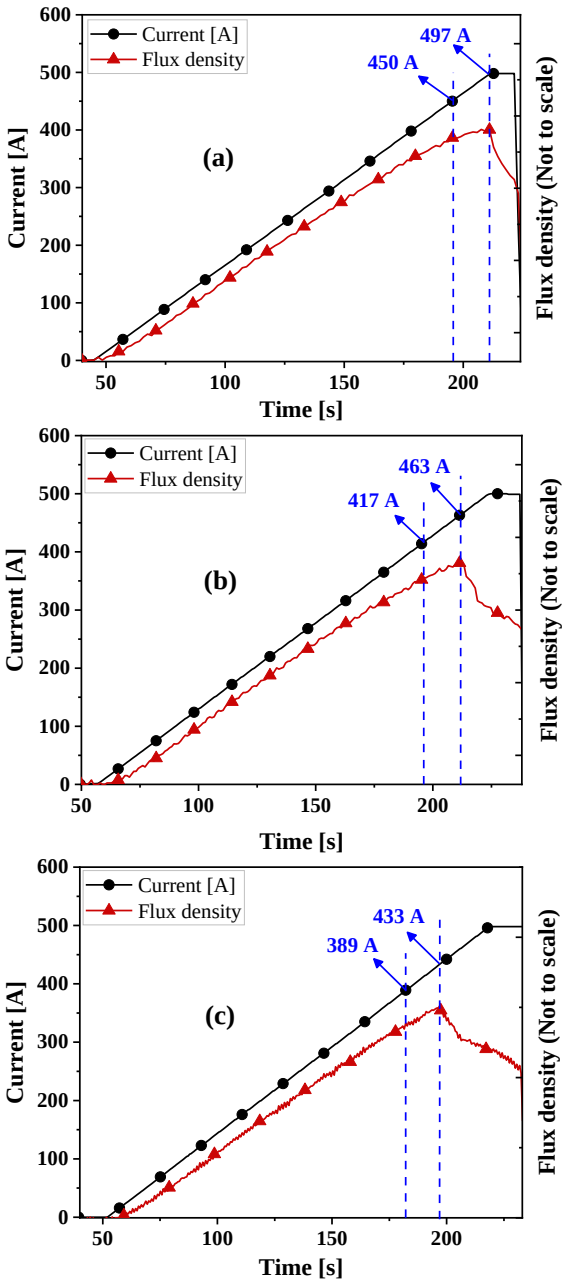

Fig. 13. Test results under external magnetic field of (a) 28.5 A_{rms} and 0.5 Hz, (b) 42.5 A_{rms} and 1 Hz, and (c) 57.6 A_{rms} and 1.5 Hz.

It is assumed that I_t (= I_{sc} + I_r, where I_{sc} and I_r represent the current flow along the spiral and radial directions, respectively) is constant value, I_r increases due to bypass current, leading to a decrease in I_{sc}. This causes a decrease in B_z value because a large amount of I_t flows along the radial direction. Further, the starting saturation of B_z under I_a= 57.6 A_{rms} and f_s= 1.5 Hz occurred at the I_t value of 389 A which was smaller than those of I_a= 28.5 A_{rms} and f_s= 0.5 Hz (450 A) and I_a= 42.5 A_{rms} and f_s= 1.0 Hz (417 A). The results demonstrated that the saturation of B_z occurred early under high strength of I_a and f_s due to bypass current phenomenon. The effects of external magnetic field on the electrical behavior of the test coil are shown in the table 3.

Figure 14 (a), (b), and (c) show the experiment temperature results according to I_a= 28.5 A_{rms} and f_s= 0.5 Hz, I_a= 42.5 A_{rms} and f_s= 1.0 Hz, and I_a= 57.6 A_{rms} and f_s= 1.5 Hz, respectively. When the external magnetic field applied to the test coil, the temperature channels A, B, and C were decreased to zero. However, the temperature channels Ch1, Ch2, and Ch7 operated normally during the test. This is because the temperature sensors were affected by the three phrase armature windings. The magnitude of this effect depends on the distance between the temperature sensors and the armature windings. Thus, the temperature channels A, B, and C were installed inside the armature windings of 75 kW class induction motor, resulting in a stronger effect than those of Ch1, Ch2, and Ch7, which were located far enough to avoid signal interference.

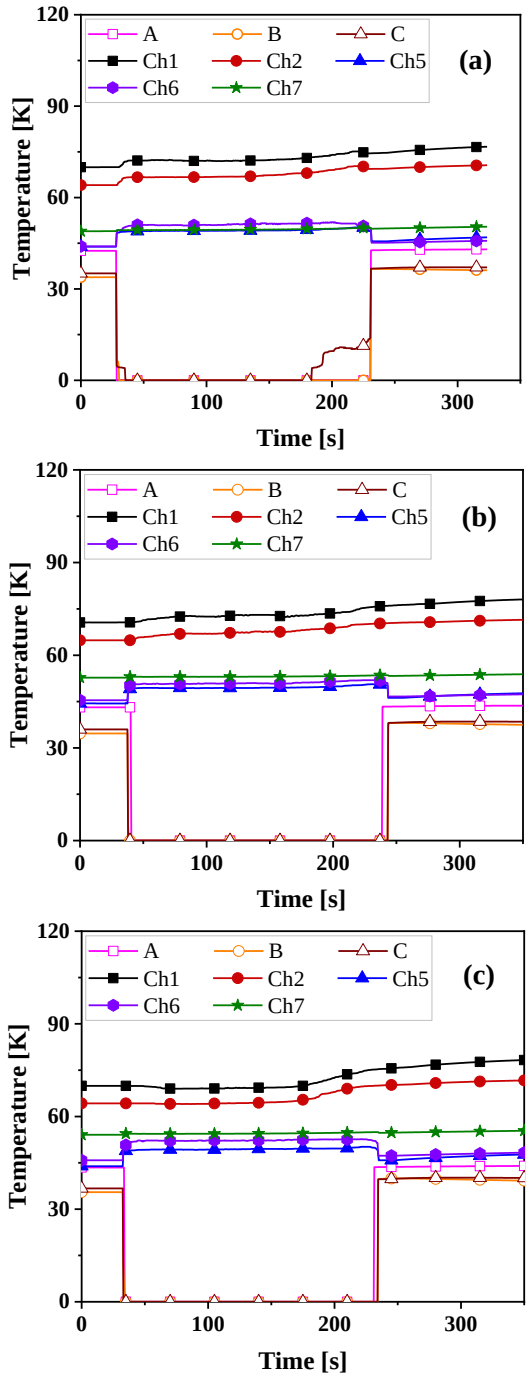

Fig. 14. Temperature results under external magnetic field of (a) 28.5 A_{rms} and 0.5 Hz, (b) 42.5 A_{rms} and 1 Hz, and (c) 57.6 A_{rms} and 1.5 Hz.

Therefore, the initial and final temperature values of these channels were utilized to estimate the influence of the external magnetic field on the temperature characteristic for the cryostat part. In general, the average increasing temperature were approximately 3.04 and 3.31 K at I_a= 28.5 A_{rms} and f_s= 0.5 Hz and at I_a= 42.5 A_{rms} and f_s= 1.0 Hz, respectively, which were smaller than that of 3.96 K at I_a= 57.6 A_{rms} and f_s= 1.5 Hz. Overall, the temperature inside cryostat part increased as the I_a and f_s of external magnetic field increased, leading to the decrease of stable operation for the test coil. Table 3 summarizes the increasing temperature at all positions inside cryostat part during the characteristic test under conduction cooling of 35 K and various AC external magnetic field.

TABLE 3
EFFECTS OF EXTERNAL MAGNETIC FIELD ON ELECTRICAL AND THERMAL CHARACTERISTICS OF THE MI-SS RACETRACK COIL UNDER CONDUCTION COOLING OF 35 K.

Channel Name	Position	Increasing temp. (K)		
		I_a= 28.5 A_{rms}, f_s= 0.5 Hz	**I_a= 42.5 A_{rms}, f_s= 1.0 Hz**	**I_a= 57.6 A_{rms}, f_s= 1.5 Hz**
A	2nd stage	0.48	0.52	0.52
B	Coil lead block	2.28	2.75	3.56
C	Coil lead block	1.96	2.47	3.30
Ch1	1st stage lead block	6.71	7.57	8.64
Ch2	1st stage lead block	6.53	6.69	7.60
Ch5	1st stage	3.08	3.36	4.01
Ch6	HTS lead	1.82	1.94	2.63
Ch7	HTS lead	1.49	1.16	1.42
AC External magnetic field		**I_a= 28.5 A_{rms}, f_s= 0.5 Hz**	**I_a= 42.5 A_{rms}, f_s= 1.0 Hz**	**I_a= 57.6 A_{rms}, f_s= 1.5 Hz**
I_t at starting decrease of B_z [A]		497	463	433
I_t at starting saturation of B_z [A]		450	417	389

4. CONCLUSIONS

In this study, we have investigated the effects of cryogenic cooling approach and rotating magnetic field on the electrical and thermal characteristics of the MI-SS racetrack coil. The conduction cooling system was successfully operated to maintain the target operating temperature of 35 and 77 K for the test coil. The charging and discharging test results demonstrated that the R_c, which is key factor affecting the τ_d and thermal stability of the test coil, decreased as the temperature cooling decreased because the generated heat inside the test coil was dissipated effectively under low temperature cooling. During the transient test under rotating magnetic field, the temperature inside the cryostat increased as the rotating magnetic field increased, resulting in a decrease of thermal stability for the test coil. In addition, when the I_a and f_s increased, the I_c value of the test coil decreased, leading to a decrease in the B_z value. Although, the test coil under conduction cooling of 35 K showed slower τ_d than those of LN_2 and conduction cooling of 77K during the charging and discharging test, the conduction cooling of 35 K effectively improved the thermal stability of the test coil under transient operation owning to high performance

cooling. Furthermore, the 3D FEA model was suggested to estimate the I_c value for the test coil under conduction cooling conditions of 35 and 77 K. The simulation results agreed well with the experiment ones, which proved that our simulation model is valid.

ACKNOWLEDGMENT

This research was supported by the 2021 scientific promotion program funded by Jeju National University.

REFERENCES

[1] J. Pelegrín *et al.*, "Numerical and experimental analysis of normal zone propagation on 2G HTS wires," *IEEE Trans. Appl. Supercond.*, vol. 21, no. 3, June. 2011, Art. no. 3041.

[2] G. Iannone *et al.*, "Quench propagation in commercial REBCO composite tapes," *Cryogenics*, vol. 109, Jul. 2020, Art. no. 103116.

[3] S. Hahn, D. K. Park, J. Bascuñán, and Y. Iwasa, "HTS pancake coils without turn-to-turn insulation," *IEEE Trans. Appl. Supercond.*, vol. 21, no. 3, pp. 1592–1595, Jun. 2011, Art. no. 1592.

[4] S. Choi, H. C. Jo, Y. J. Hwang, S. Hahn, and T. K. Ko, "A study on the no insulation winding method of the HTS coil," *IEEE Trans. Appl. Supercond.*, vol. 22, no. 3, Jun. 2012, Art. no. 4904004.

[5] X. Wang *et al.*, "Turn-to-turn contact characteristics for an equivalent circuit model of no-insulation ReBCO pancake coil," *Supercond. Sci. Technol.*, vol. 26, no. 3, Jan. 2013, Art. no. 035012.

[6] Y-G Kim *et al.*, "Numerical analysis on bifurcated current flow in no-insulation magnet," *IEEE Trans. Appl. Supercond.*, vol. 24, no. 3, Jun. 2014, Art. no. 4900404.

[7] T. Wang, "Analyses of transient behaviors of no-insulation REBCO pancake coils during sudden discharging and overcurrent," *IEEE Trans. Appl. Supercond.*, vol. 25, no. 3, Jun. 2015, Art. no. 4603409.

[8] H. L. Quach *et al.*, "Analytical and numerical simulation on charging behavior of no-insulation REBCO pancake coil," *Prog. Supercond. Cryog.*, vol. 20, no. 4, pp. 16 – 19, Dec. 2018.

[9] H. L. Quach, "Analysis on electrical and thermal characteristics of a no-insulation HTS coil considering heat generation in steady and transient states," *IEEE Trans. Appl. Supercond.*, vol. 29, no. 5, Aug. 2019, Art. no. 4701506.

[10] T. S. Lee *et al.*, "The effects of co-wound kapton, stainless steel and copper, in comparison with no insulation, on the time constant and stability of GdBCO pancake coils," *Supercond. Sci. Technol.*, vol. 27, no. 6, May. 2014, Art. no. 065018.

[11] D. G. Yang, Y. H. Choi, Y. G. Kim, J. B. Song, and H. G. Lee, "Analytical and experimental investigation of electrical characteristics of a metallic insulation GdBCO coil," *Rev. Sci. Instrum.*, vol. 87, no. 3, Feb. 2016.

[12] S. Noguchi *et al.*, "Numerical investigation of metal insulation technique on turn-to-turn contact resistance of REBCO pancake coils," *IEEE Trans. Appl. Supercond.*, vol. 27, no. 4, Jun. 2017, Art. no. 7700505.

[13] D. G. Yang *et al.*, "A study on electrical characteristics of multilayered metallic-insulation coils," *IEEE Trans. Appl. Supercond.*, vol. 27, no. 4, Jun. 2017, Art. no. 7700206.

[14] M-H Sohn *et al.*, "Controllability of the contact resistance of 2G HTS coil with metal insulation," *IEEE Trans. Appl. Supercond.*, vol. 28, no. 3, Apr. 2018, Art. no. 4602705.

[15] Y. S. Chae *et al.*, "Design and analysis of HTS rotor-field coils of a 10-MW-class HTS generator considering various electric insulation techniques," IEEE Trans. Appl. Supercond., vol. 30, no. 4, Jun. 2020, Art. no. 4601707.

[16] H. L. Quach and H. M. Kim, "A study on charging and electrical stability characteristics with no-insulation and metal insulation in form of racetrack type coils," *Prog. Supercond. Cryog.*, vol. 22, no. 3, pp. 13–19, Sep. 2020.

[17] H. L. Quach *et al.*, "Effects of stainless steel thickness and winding tension on electrical and thermal characteristics of metal insulation racetrack coils for 10-MW-class HTS wind generator," *Cryogenics*, vol. 115, Apr. 2021, Art. no. 103256.